Equilibrium polymerization and gas-liquid critical behavior in the Stockmayer fluid

Reinhard Hentschke,* Jörg Bartke, and Florian Pesth†
Fachbereich Mathematik und Naturwissenschaften, Bergische Universität, D-42097 Wuppertal, Germany
(Received 16 October 2006; revised manuscript received 7 December 2006; published 25 January 2007)

We develop a simple theory explaining the dependence of the gas-liquid critical point in the Stockmayer fluid on dipole strength. The theory is based on the Flory-Huggins lattice description for polymer systems in conjunction with a transfer matrix model for isolated chains of reversibly assembled dipolar particles. We find that the shift of the critical point as a function of dipole strength, which originally was found in computer simulation, strongly resembles the critical point shift as a function of chain length in ordinary linear polymer systems. In particular, the decrease of the critical density with increasing dipole strength is a consequence of the existence of reversible chains near criticality. In addition we report simulation results for gas-liquid critical points well above the limiting dipole strength found previously.

DOI: 10.1103/PhysRevE.75.011506 PACS number(s): 64.70.Fx, 82.35.−x, 05.50.+q

I. INTRODUCTION

The addition of dipolar interaction to short-range potentials used to describe simple liquids leads to new complex phase behavior depending on the dipole strength and other variable details of the microscopic models. Most theoretical and simulation work has focused on gas-liquid coexistence and on the Curie-Weiss-like isotropic-to-nematic liquid transition [1,2]. Dipolar liquids are of interest to researchers in quite distinct fields like low-molecular-weight liquids or liquid crystals, colloidal ferrofluids, and polymers. This is because dipolar interaction may lead to the reversible formation of polydisperse chains from molecules or colloidal particles [3] (see in particular Ref. [1] and the references therein) whose physical behavior is similar to that of ordinary polymer systems [4]. The chain formation in turn strongly affects the behavior of the monomer systems. This coupling, together with the special problems caused by long-range interaction, thus far has prevented a complete theory, particularly for computing the phase diagram of dipolar liquids.

Here we focus on the coupling between gas-liquid critical behavior and the formation of reversible dipole chains in Stockmayer fluids (SFs). In the latter the particles interact via a normal 12-6 Lennard-Jones (LJ) potential plus a dipole-dipole potential between point dipoles $\vec{\mu}$ located on the LJ sites. The Stockmayer potential is one of three potentials used extensively to model dipolar fluids. The other two are the dipolar soft sphere potential, which neglects the LJ attraction in the SF, and the dipolar hard sphere (DHS) potential, which posses a hard core instead of the SF's LJ potential. All three models have been shown to exhibit ferroelectric liquid order under suitable conditions (see Ref. [5] for a detailed discussion). However, with respect to gas-liquid phase separation they differ. The SF is based on the LJ potential, and therefore it will phase separate even for vanishing dipole moments. For models without dispersion attraction this is a prior unclear. For the DHS model the existence of gas-liquid phase separation still is under debate [1,2]. Based on simulation work van Leeuwen and Smit [6] had concluded that gas-liquid phase separation depends on the strength of the dispersion attraction. They had investigated a modified SF in which the r^{-6} term is replaced by λr^{-6}, where λ varies between 0 and 1. Notice that $\lambda=0$ corresponds to the soft sphere potential. Below $\lambda\approx 0.3$ they did not find gas-liquid phase separation, which they attributed to chain formation. This claim was supported by theoretical work (e.g., [7,8]) showing that chains of DHSs essentially should not interact. Because the modified SF of Ref. [6] can be mapped onto the ordinary SF, it was concluded [9] that the ordinary SF will not show gas-liquid phase separation for dipole moments exceeding $\mu\approx 5$. A different conclusion was reached by Dudowicz, Freed, and Douglas [10], who map the Stockmayer fluid onto a Flory-Huggins (FH) mean-field lattice model. Their theory implies that the gas-liquid critical point exists for all dipole strength.

The basis of our theory, i.e., the FH lattice description, is the same as in Refs. [10–12]. However, we do choose a different mapping between the lattice model's direct interaction parameters and the Stockmayer fluid. Our approach allows us to directly relate the shift of the gas-liquid critical point to the details of the underlying interactions. In agreement with Ref. [10] our theory does not yield evidence for the disappearance of gas-liquid criticality at large finite dipole strengths reported previously. This finding is supported by the results of molecular dynamics computer simulations. Using the simple Maxwell construction method we do observe gas-liquid criticality well beyond the above limiting dipole strength in good accord with our theory. We also stress the similarity between the mean-field critical behavior in this system in comparison to ordinary systems of linear polymers.

II. FLORY-HUGGINS MODEL FOR REVERSIBLY ASSEMBLING POLYMERS

In Ref. [13] we had introduced the following free energy of an N-site lattice with variable occupation, i.e., including empty sites:

*Author to whom correspondence should be addressed. Electronic address: hentschk@uni-wuppertal.de
†Present address: Physics Department, Johannes Gutenberg University, D-55988 Mainz, Germany.

$$\frac{b_0 F_L}{VT} = \frac{1}{2} q\varepsilon_{MM}\phi_1^2 + \frac{1}{2} q\varepsilon_{AA}\phi_{agg}^2 + q\varepsilon_{MA}\phi_1\phi_{agg} + \sum_{s=1}^{\infty} \frac{\phi_s}{s} \ln\left(\frac{\phi_s}{s}\right) + (1-\phi)\ln(1-\phi) + (c+1)\sum_{s=2}^{\infty}\left(\frac{s-1}{s}\right)\phi_s, \tag{1}$$

where $c=\varepsilon_i-\ln[q-1]$. In this equation the terms explicitly containing the parameters ε_{xy} and ε_i constitute the contact interaction part of the free energy. The other terms account for the packing entropy proportional to the logarithm of the number of ways s-mers can be distributed on the lattice leaving a certain number of sites empty. Here 1-mers are free solute monomers (index M) occupying a single lattice site, and s-mers ($s>1$) are reversible linear aggregates (index A) formed by monomers. The ε_{xy} parameters are the contact free energies of occupied sites of type x and y, respectively, whereas ε_i describes the monomer-monomer interactions within aggregates. The ϕ_s are the volume fractions of the respective particles. Note that $\phi_s=b_0 s N_s/V$, $\phi=\Sigma_{s=1}^{\infty}\phi_s$, and $N=\Sigma_{s=1}^{\infty} sN_s+N_{empty}$, where N_s is the number of s-mers, N_{empty} is the number of empty sites, and b_0 is the site volume. In addition $q=6$ is the coordination number of the cubic lattice. Here, in comparison to Ref. [13], we do omit additional solvent particles. In the following we also drop the distinction between the ε_{xy} parameters replacing each ε_{xy} by a single ε [14]. The resulting lattice free energy becomes

$$\frac{b_0 F_L}{VT} = \frac{1}{2} q\varepsilon\phi^2 + \sum_{s=1}^{\infty} \frac{\phi_s}{s} \ln\left(\frac{\phi_s}{s}\right) + (1-\phi)\ln(1-\phi) + (c+1)\sum_{s=2}^{\infty}\left(\frac{s-1}{s}\right)\phi_s. \tag{2}$$

Using the equilibrium condition $\mu_s=s\mu_1$, where $\mu_s=(\partial F_L/\partial N_s)_{T,V,N_{s'(s'\neq s)}}$ is the chemical potential of an s-mer, we obtain $\phi_s=s\beta^s e^c$ with $\beta=\phi_1 e^{-c}$. Together with the mass conservation condition $\phi=\phi_1+\phi_{agg}$, the mean particle size n becomes

$$n = \frac{\sum_{s=1}^{\infty}\phi_s}{\sum_{s=1}^{\infty}\phi_s/s} = \frac{1}{1-\beta}. \tag{3}$$

Notice that we may combine this equation with the mass conservation condition to yield n expressed via ϕ, i.e.,

$$n = \frac{1}{2} + \frac{1}{2}\sqrt{1+4(q-1)\phi e^{-\varepsilon_i}}. \tag{4}$$

The equation of state follows via $P=-(\partial F_L/\partial V)_{T,N_s}$, i.e.,

$$\frac{b_o P}{T} = -\left(1-\frac{1}{n}\right)\phi + \frac{1}{2} q\varepsilon\phi^2 - \ln(1-\phi), \tag{5}$$

using $\phi_{agg}=(1-n^{-2})\phi$. This result coincides with the equation of state for monodisperse polymers of fixed length n. Here, however, n is a function of ϕ. We therefore obtain for the gas-liquid critical point

$$\phi_c = f_\rho(n_c) = \begin{cases} \frac{1}{2} - \frac{3}{4}(n_c-1)^2 + O((n_c-1)^3) & n_c \to 1, \\ \frac{\sqrt{3}}{2}\frac{1}{n_c^{1/2}} - \frac{3}{4}\frac{1}{n_c} + O\left(\frac{1}{n_c^{3/2}}\right) & n_c \to \infty, \end{cases} \tag{6}$$

$$T_c = -q\varepsilon_0 f_T(n_c) = \begin{cases} \frac{-q\varepsilon_0}{4}[1+(n_c-1)+O((n_c-1)^2)] & n_c \to 1, \\ -q\varepsilon_0\left(1-\frac{5}{2\sqrt{3}}\frac{1}{n_c^{1/2}}+O\left(\frac{1}{n_c}\right)\right) & n_c \to \infty, \end{cases} \tag{7}$$

and

$$b_0 P_c = \begin{cases} -q\varepsilon_0\left[\left(\frac{\ln 2}{4}-\frac{1}{8}\right)+O(n_c-1)\right] & n_c \to 1, \\ -q\varepsilon_0\left[\frac{5\sqrt{3}}{16}\frac{1}{n_c^{3/2}} - \frac{77}{64}\frac{1}{n_c^2} + O\left(\frac{1}{n_c^{5/2}}\right)\right] & n_c \to \infty. \end{cases} \tag{8}$$

Here $\varepsilon=\varepsilon_0/T$, $n_c=n(\phi_c,\varepsilon_i(T_c))$,

$$f_\rho(n) \equiv \left(1+\sqrt{\frac{m^3}{K}}\right)^{-1}, \tag{9}$$

where $m=2n-1$ and $K=6n(n-1)+1$, and

$$f_T(n) \equiv \frac{1}{2}\left(\frac{n}{m} + [K-n(n-1)]\sqrt{\frac{1}{Km^3}}\right)^{-1}. \tag{10}$$

For large n_c the critical density vanishes as $\sim n_c^{-1/2}$, whereas the critical temperature approaches a constant value, which coincides with the Boyle temperature of the monomer system.

In this theory reversible association is promoted by the quantity ε_i. In particular, $\varepsilon_i=0$ describes the limit of an ordinary simple liquid. For $\varepsilon_i=0$ and $q=6$, however, one obtains $n_c=(\sqrt{11}+1)/2\approx 2.158$ and not $n_c=1$ as one may expect. This theory reaches the limit $n_c=1$ only if $\exp(-c)=0$. But this means that $n_c=1$ under all circumstances, i.e., no association occurs even if $\varepsilon_i\neq 0$. The effect is due to the inability of the lattice theory to distinguish between adjacent unassociated and reversibly bound lattice sites. Because of this we must redefine the simple liquid (SL) limit, i.e., $\varepsilon_i=0$, via the simultaneous solution of Eqs. (4) and (6) given by $n_{c,SL}\approx 2.0142$ and $\phi_{c,SL}=f_\rho(n_{c,SL})\approx 0.4086$. The attendant critical temperature is $T_{c,SL}=-q\varepsilon_{0,SL}f_T(n_{c,SL})\approx -0.4002 q\varepsilon_{0,SL}$.

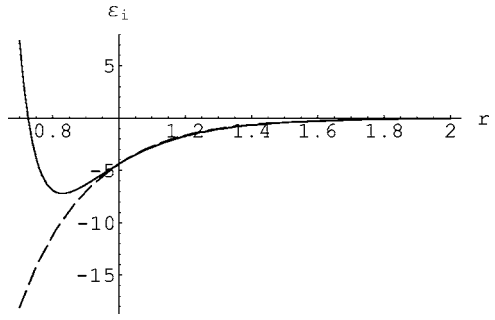

FIG. 1. Comparison of ε_i according to the expression in square brackets in Eq. (24) (solid line) to ε_i according to the expression in square brackets in Eq. (25) (dashed line) plotted vs r for $T=10$ and $\mu^2=36$. Note that $\varepsilon_i(\mu^2/(Tr_0^3)) \approx -9.7$ [using Eq. (25)] and $r_0 \approx 0.73$ in this special case.

This theory can explain the decrease of the critical density with increasing dipole strength μ^2, in terms of an increasing mean particle size n. Thus we must find a link between μ^2 and n. We start by introducing μ^2 on the level of the equation of state, i.e., we approximately include the pressure contribution due to long-range dipolar attractive interaction via

$$P_{DD} \approx -\frac{1}{6}\rho^2 \int_{r \geqslant R} d^3r\, r \frac{\partial \langle u_{DD} \rangle}{\partial r} = -\frac{8\pi}{9}\frac{\mu^4 \rho^2}{TR^3}, \tag{11}$$

where $\langle u_{DD} \rangle = -2\mu^4/(3Tr^6)$ is the thermally averaged dipole-dipole interaction energy [assuming $-\mu^2/(Tr^3) \ll 1$; units are: $T := Tk_B/\epsilon$, $r := r/\sigma$, and $\mu^2 := \mu^2/(4\pi\epsilon_0\epsilon\sigma^3)$, where k_B is Boltzmann's constant, ϵ_0 is the vacuum permitivity, and ϵ and σ are the usual LJ-parameters, which in the following set the units energy and length]. Here r is the dipole-dipole separation, and R is a suitable cutoff. We integrate this contribution into the equation of state (5) via the substitution

$$\varepsilon_0 = \varepsilon_{0,SL} - \frac{16\pi}{9qb_0R^3}\frac{\mu^4}{T}. \tag{12}$$

Inserting this equation into Eq. (7) yields

$$T_c(\mu) \propto \mu^2 \quad \text{for } \mu^2 \to \infty,$$

$$T_c(\mu) = T_{c,SL} \quad \text{for } \mu^2 = 0, \tag{13}$$

at fixed n_c. This is in reassuring agreement with simulation data shown in Fig. 3. We note that the applicability of Eq. (11) rests on the premise that the individual dipoles retain sufficient rotational freedom even as part of a reversible chain.

Next we consider the lattice free energy in the limit of a single infinitely long chain and vanishing ϕ_{agg}, i.e.,

$$\frac{F_L}{sT} = \varepsilon_i - \ln(q-1). \tag{14}$$

In order to find an approximate expression for $\varepsilon_i = \varepsilon_i(\mu^2)$ we estimate the configuration free energy of an isolated chain consisting of s Stockmayer dipoles based on the potential energy

$$U^{(chain)} = \sum_{i=1}^{s-1} [u_{LJ}(r_{i,i+1}) + \vec{\mu}_i \mathbf{T} \vec{\mu}_{i+1}], \tag{15}$$

where u_{LJ} is the LJ pair potential and $\mathbf{T}$ is the dipole tensor. The summation includes the interaction of immediate neighbors only, which in the one-dimensional case is not unreasonable. In addition we assume a uniform "bond length" $r = |\vec{r}_{i,i+1}|$. The configurational partition function now becomes

$$Q_{conf}^{(chain)} = \int d\{\Omega_{\vec{r}}\} d\{\Omega_{\vec{\mu}}\} \exp\left(-\frac{1}{T}U^{(chain)}\right). \tag{16}$$

We want to evaluate the integration on a simple cubic lattice, i.e.,

$$\int d\{\Omega_{\vec{r}}\} d\{\Omega_{\vec{\mu}}\} \approx \left(\frac{4\pi}{q}\right)^{2s-1} \sum_{\{\Omega_{\vec{r}}\},\{\Omega_{\vec{\mu}}\}}. \tag{17}$$

Note that there are s dipole moments connected by $s-1$ bonds. The chain becomes a path on the cubic lattice ($q=6$). Every lattice site on the path is occupied by a dipole $\vec{\mu}_i$ oriented along one of six possible lattice directions. The possible orientations are given by the vectors $\vec{e}^{(1)}=(1,0,0)$, $\vec{e}^{(2)}=(0,1,0)$, $\vec{e}^{(3)}=(0,0,1)$, $\vec{e}^{(4)}=-\vec{e}^{(1)}$, $\vec{e}^{(5)}=-\vec{e}^{(2)}$, and $\vec{e}^{(6)}=-\vec{e}^{(3)}$, i.e., $\vec{\mu}^{(k)}=\mu\vec{e}^{(k)}$. Because every segment along the chain contributes the same to the total LJ interaction we may write this factor in front of the sum and replace the sum by the following trace:

$$Q_{conf}^{(chain)} = \exp[-(s-1)u_{LJ}(r)/T]\mathrm{Tr}(\mathbf{M}^{s-1}\mathbf{M}_0), \tag{18}$$

where

$$M_{kl} = \sum_{\nu=1}^{6} \exp\left(-\frac{1}{T}\sum_{\alpha,\beta} \mu_\alpha^{(k)} T_{\alpha\beta}^{(\nu)} \mu_\beta^{(l)}\right) \tag{19}$$

$(k,l=1,\ldots,6)$ are the elements of a transfer matrix $\mathbf{M}$, and $T_{kl}^{(\nu)}$ are the components of the dipole tensor

$$T_{\alpha\beta}^{(\nu)} = \frac{1}{r^3}(\delta_{\alpha\beta} - 3e_\alpha^{(\nu)} e_\beta^{(\nu)}). \tag{20}$$

The elements of the matrix $\mathbf{M}_0$ are simply all equal to 1. We obtain for the configuration free energy of the chain

$$\frac{1}{sT}F_{conf}^{(chain)} \approx \frac{s-1}{s}\min_r\left(u_{LJ}(r)/T - \ln\frac{\lambda_{max}(r)}{q^2}\right) - \frac{2s-1}{s}\ln 4\pi, \tag{21}$$

where λ_{max} is the largest eigenvalue of $\mathbf{M}$ given by

$$\lambda_{max}(r) = 2e^{2a}(1 + 2e^{-a} + 12e^{-2a} + 2e^{-3a} + e^{-4a}) \tag{22}$$

with

$$a = \frac{\mu^2}{\mathrm{Tr}^3}. \tag{23}$$

Note that $\min_r$ accounts for the fact that r is a variable parameter. Comparing Eq. (14) with Eq. (21) we find that ε_i is given by

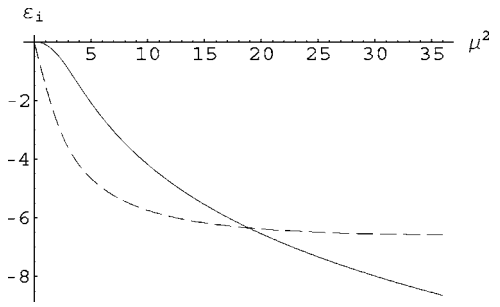

FIG. 2. Based on the theoretical curves shown in Fig. 3 this plot compares $\varepsilon_i[\mu^2/(T_c r_0^3)]$ (solid line) at the critical point with the simple approximation $-2\mu^2/T_c$ (dashed line).

$$\varepsilon_i \approx \left[\frac{1}{T}u_{LJ}(r) - \ln \lambda_{max}(r) + 2 \ln q\right]_{r=r_{min}}, \tag{24}$$

where we have replaced $(s-1)/s$ by unity. Here r_{min} is the separation for which the expression (24) acquires its minimum. Note also that the term $(2s-1)/s \ln(4\pi)$ that appears in Eq. (21) is missing here. This is because a factor $s \ln(4\pi)$, corresponding to the dipole orientation, is not present in the lattice free energy. The remaining part, $(s-1)\ln(4\pi)$, corresponds to the orientation of the bonds in the off-lattice case, which in the lattice model is replaced by the term $\ln(q-1)$. Notice that for $\mu^2=0$ we find $\varepsilon_i \approx u_{LJ}(r_{min})/T$. Because the LJ fluid is our simple liquid we must not use (24) directly but rather

$$\varepsilon_i \approx [-\ln \lambda_{max}(r) + 2 \ln q]_{r=r_{min}}, \tag{25}$$

where r_{min} is the optimal monomer separation within a chain computed via minimization of expression (24).

The last ingredient to our theory of the μ^2 dependence of the critical point is the relation

$$b_0 \approx b_{0,SL}\frac{r_0}{r_{0,SL}}. \tag{26}$$

Here r_0 is the root of expression (24), and $r_{0,SL}=1$ is the root of the same expression in the limit $\mu^2=0$. Because the dipolar interaction within a chain leads to an attraction increasing with increasing μ^2, we do see from Eq. (6) that at constant n_c this leads to an increase of the critical monomer number density $\rho_c=\phi_c/b_0$. However, if n_c is increasing with increasing μ^2 then the competition of the two effects will determine $\rho_c(\mu^2)$.

The two quantities r_{min} and r_0 are illustrated in Fig. 1, which shows the dependence of the expression (24) on r for $T=10$ and $\mu^2=36$. The minimum of this expression (solid line) yields r_{min} and the function $-\ln \lambda_{max}(r)+2 \ln q$ (dashed line) evaluated at $r=r_{min}$ is $\varepsilon_i(\mu^2/(Tr_{min}^3)) \approx -9.7$ for this temperature and dipole strength. In addition $r_0 \approx 0.73$ is the root of expression (24) in this special case. Figure 2 shows the comparison of $\varepsilon_i[\mu^2/(T_c r_{min}^3)]$ plotted vs dipole strength with the simple approximation $-2\mu^2/T_c$. We note that the simple approximation comes close to being constant for $\mu^2 > 10$.

In order to compute the critical point shift as function of μ^2 together with the critical aggregation number n_c, we need to solve Eqs. (4), (6), and (7) using Eqs. (12), (25), and (26). Introducing the definitions $x_\rho \equiv \rho_c/\rho_{c,SL}$ and $x_T \equiv T_c/T_{c,SL}$ we may rewrite the above set of equations, i.e., Eqs. (4), (6), and (7), in a more transparent form:

$$n_c = \frac{1}{2} + \frac{1}{2}\sqrt{1 + 4(q-1)e^{-\varepsilon_i} f_\rho(n_c)}, \tag{27}$$

$$x_\rho \approx \frac{f_\rho(n_c)}{r_0 f_\rho(n_{c,SL})}, \tag{28}$$

$$\frac{1}{x_T}\left(1 + \frac{\kappa\mu^4}{r_0}\frac{1}{x_T}\right) \approx \frac{f_T(n_{c,SL})}{f_T(n_c)}, \tag{29}$$

where $\kappa = 16\pi\rho_{c,SL} f_T(n_{c,SL})/[9R^3 T_{c,SL}^2 f_\rho(n_{c,SL})]$, $r_0 = r_0(\mu^2, T_c)$, and $\varepsilon_i = \varepsilon_i[\mu^2/(T_c r_{min}^3)]$. Here $\rho_{c,SL}$ and $T_{c,SL}$ are the respective values for the LJ system.

We want to discuss this result before comparing it to computer simulation. Assuming for the moment that r_{min} and r_0 are constants, we do observe that x_ρ or ρ_c will simply decrease if the average critical chain length increases at T_c. We do expect an increase of n_c because for small dipole strength μ^2 increases faster than T_c as Eq. (29) shows. However, for long chains $f_T(n_c)$ approaches 1 and $T_c \propto \mu^2$. This in turn implies that ε_i becomes constant, which means that n_c and thus also ρ_c approaches a constant. This basic behavior, i.e., an initial slow increase of T_c, as function of μ^2, which subsequently will be steeper and proportional to μ^2 and the decrease of ρ_c which then levels off as soon as $T_c \propto \mu^2$, is modified by the μ^2 dependence of r_{min} and r_0. A decrease of r_{min} with increasing μ^2 promotes growth because it tends to increase the magnitude of ε_i. This will decrease $f_\rho(n_c)$ causing ρ_c to decrease. On the other hand the factor $1/r_0$ in Eq. (28) will counteract this decrease to some extent. In the following section we analyze this dependence numerically.

III. COMPARISON TO MOLECULAR DYNAMICS SIMULATION RESULTS

Figure 3 compiles and compares simulation results for the gas-liquid critical temperature T_c and the critical density ρ_c of the Stockmayer fluid plotted versus dipole strength μ^2. The star symbols denote data points obtained by this group using molecular dynamics simulations in conjunction with the Maxwell construction method to determine the coexisting gas and liquid densities. We carry out a large number of *NVT* simulations along an isotherm which allows us to employ the Maxwell construction to obtain the coexisting densities of the pure gas and the pure liquid. Note that the system was compressed and subsequently expanded to check for hysteresis. Repeating this procedure for a series of temperatures yields the gas-liquid coexistence curve, which we analyze using the well-known scaling relations to extract the critical point data. For selected dipole strengths the resulting binodal lines were confirmed using thermodynamic integration (Kofke's method). These simulations are described in detail

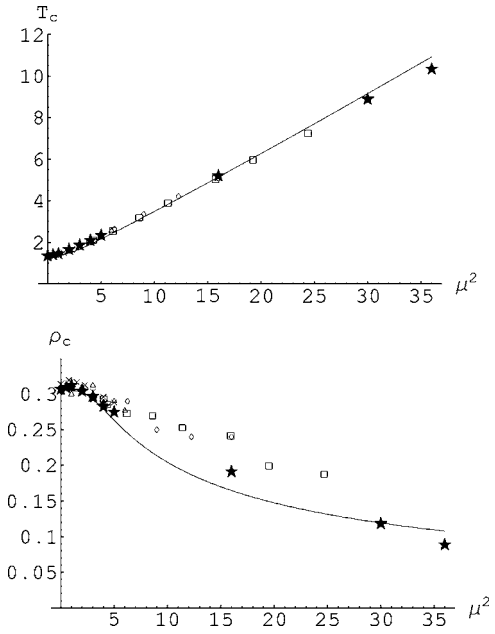

FIG. 3. Top: Gas-liquid critical temperature T_c of the Stockmayer fluid vs dipole strength μ^2. Symbols indicate computer simulation results (stars, this group); hollow squares, Ref. [6]; hollow diamonds, Ref. [9]; hollow triangles, Ref. [16]; crosses, Ref. [17]). Bottom: Gas-liquid critical density ρ_c of the Stockmayer fluid vs dipole strength μ^2. The solid lines are the theoretical result obtained for $R=4.1$.

elsewhere [15]. All other symbols denote previously published data by other groups [6,9,16,17]. Notice that the data taken from Ref. [6] were mapped via the relations $T_{ST}=\lambda^{-2}T_{vLS}$, $\rho_{ST}=\lambda^{-1/2}\rho_{vLS}$, and $\mu_{ST}=\lambda^{-3/4}\mu_{vLS}$ (cf. Sec. II in Ref. [9]). These relations transform the potential considered in Ref. [6] (vLS), i.e.,

$$\frac{U_{vLS}(r_{vLS},\mu_{vLS})}{T_{vLS}} = \frac{4}{T_{vLS}}\left(\frac{1}{r_{vLS}^{12}} - \lambda\frac{1}{r_{vLS}^{6}}\right) - \frac{\mu_{vLS}^2}{T_{vLS}r_{vLS}^3}f, \tag{30}$$

where f simply is a function of the relative orientation of two interacting dipoles, to the Stockmayer potential (ST), i.e.,

$$\frac{U_{ST}(r_{ST},\mu_{ST})}{T_{ST}} = \frac{4}{T_{ST}}\left(\frac{1}{r_{ST}^{12}} - \frac{1}{r_{ST}^{6}}\right) - \frac{\mu_{ST}^2}{T_{ST}r_{ST}^3}f. \tag{31}$$

It is worth noting that the authors of Ref. [6], using Gibbs ensemble Monte Carlo simulations, were unable to observe gas-liquid coexistence for $\lambda<0.3$, which for the Stockmayer potential corresponds to $\mu^2>24$. It is also worth noting that the above mapping allows us to interpret the limit when isotropic attraction becomes vanishingly small in terms of the ordinary Stockmayer fluid in the limit of large dipole moments.

The theoretical curves are obtained by numerical solution of Eqs. (27)–(29) computing ε_i according to Eq. (25) using r_0 obtained via the minimization condition (24). Here we use the LJ critical constants, $\rho_{c,SL}=0.305$ and $T_{c,SL}=1.32$. The only adjustable parameter is the cutoff radius R in Eq. (11), which is set to $R=4.1$. The resulting agreement with the simulation results for T_c vs μ^2 shown in Fig. 3 (top panel) is excellent. The bottom panel of Fig. 3 shows the theoretical ρ_c vs μ^2 (again for $R=4.1$) in comparison to the simulation results. We do find quite reasonable agreement between the theory and our simulations over the entire range of dipole strengths. However, both our theory and the simulations yield critical densities which are systematically lower than the values obtained previously with the Gibbs ensemble molecular dynamics (GEMD) method in the range $\mu^2>5$. In addition, and more important, we do observe gas-liquid criticality for $\mu^2=30$ and $\mu^2=36$. This is well above the limit discussed previously beyond which the gas-liquid critical point should disappear.

It is worth pointing out that an equally good result for T_c vs μ^2 may be obtained by simply adding the pressure contribution (11) to any simple monomer equations of state [for instance Eq. (5) with $n=1$ or the van der Waals equation of state]. It is the decrease of the critical density with increasing μ^2 which presents a challenge. In the case of Eq. (5) with $n=1$ or the van der Waals equation the critical density is inversely proportional to the monomer volume. In order for the critical density to drop this volume must effectively increase. The reversible aggregation of monomers into linear chains offers a simple mechanism as shown by Eq. (6). Even though the FH-type lattice model employed here is not difficult, there is an even simpler way to understand this point intuitively. Let b describe the volume parameter in the van der Waals equation. Then, as just mentioned, the critical (chain) number density ρ_c^{chain} is proportional to b^{-1}, i.e., $\rho_c^{chain}\propto b^{-1}$. If now a reversible chain consisting of n monomers can be treated as an "ideal coil" or "blob" with a mean diameter $\sim n^{1/2}$ and therefore with $b\sim n^{3/2}$ interacting with other such blobs the resulting critical density of this fluid of blobs obeys $\rho_c^{chain}\sim n^{-3/2}$. Multiplying ρ_c^{chain} with n we obtain for the monomer number density $\rho_c\sim n^{-1/2}$. This is exactly the same scaling behavior as in Eq. (6) for large n_c. The problem with this simple van der Waals picture is that there usually is significant overlap between blobs at the densities of interest. For instance, we can extend the scaling argument to the critical temperature, which in the van der Waals case is proportional to a/b, where a is the attraction parameter. Using $a\propto n^2$ we obtain $T_c\propto n^{1/2}$, i.e., the critical temperature does not approach a finite value as $n\to\infty$. In the case at hand this yields an exaggerated rise of T_c with increasing μ^2.

The existence of chains near the gas-liquid critical point is illustrated pictorially in Fig. 4. The figure shows two snapshots taken during a molecular dynamics simulation of 2048 Stockmayer particles with $\mu^2=36$ near the critical density. The upper panel shows a system configuration at a temperature high enough to suppress chain formation. The lower panel corresponds to $T\approx T_c$. In this case chain segments are clearly discernible.

The preceding theoretical analysis of the critical point shift attributes the decreasing critical density to a corresponding increase of the average chain lengths. In order to support this point Fig. 5 shows the dependence of the average chain length at criticality, obtained from MD simulations, on dipole strength. Two Stockmayer particles are considered to be neighbors along a chain if their distance is less

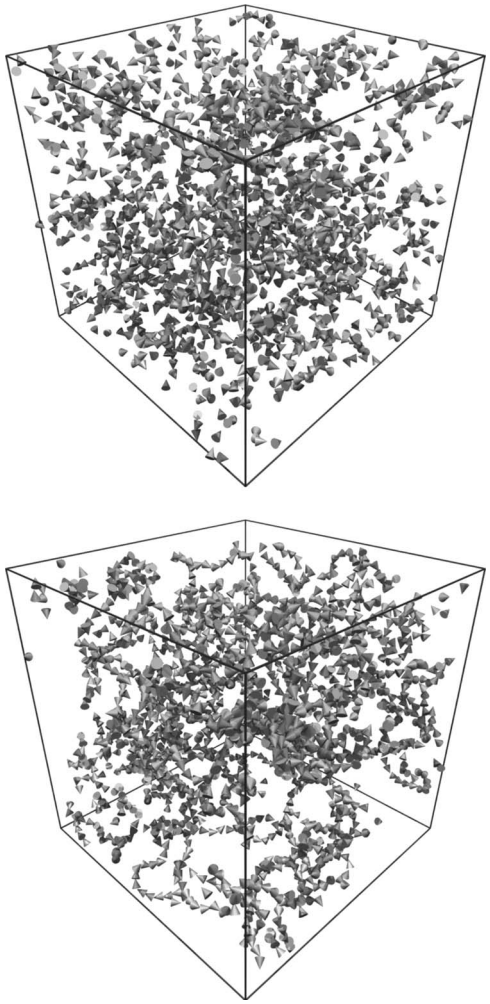

FIG. 4. Snapshots taken during a molecular dynamics computer simulation of 2048 Stockmayer particles with $\mu^2=36$ at $\rho=0.099$ ($\approx\rho_c$). Top: $T=14.0$; bottom: $T\approx T_c$. Each Stockmayer particle is represented by a cone oriented along the instantaneous direction of the particle's dipole moment.

than r_n. This is a very simple criterion and consequently the average chain length depends considerably on the value of r_n. More complicated criteria combine distance, dipole orientation, and interaction energy. Nevertheless, we do observe

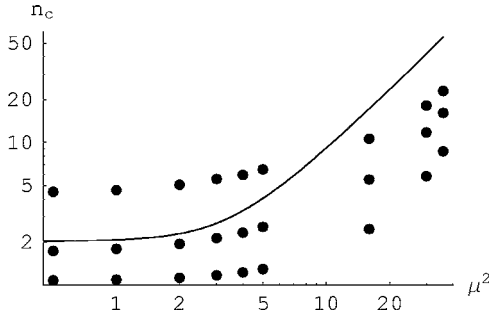

FIG. 5. Mean critical aggregation number n_c vs dipole strength μ^2. Solid circles, MD simulation analyzed with $r_n=1.0$ (bottom), 1.1 (middle), 1.2 (top); solid line, theoretical results corresponding to the theoretical curves in Fig. 3.

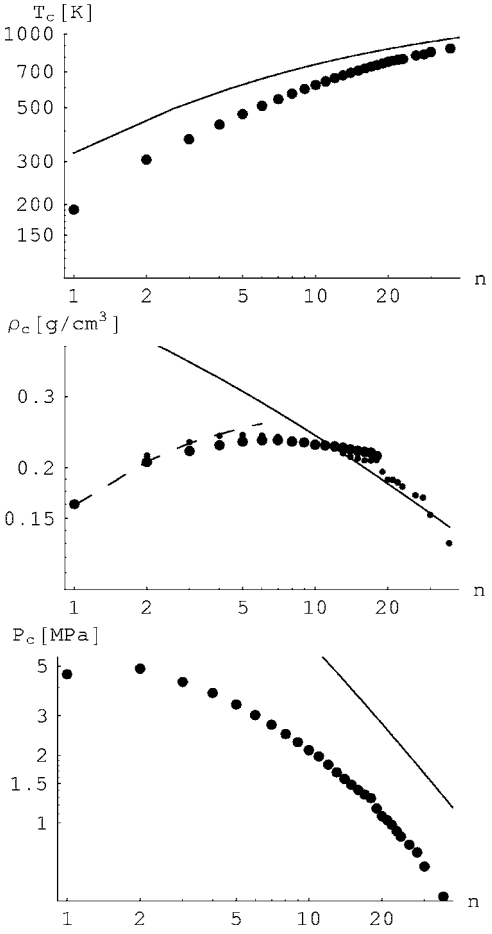

FIG. 6. The critical point of n-alkanes as function of n. Large dots, experimental critical point data for n-alkanes taken from Table 2 in Ref. [18] vs the number of methylene groups, n: small dots, critical density computed via $\rho_c=6.718nP_c/T_c$; solid lines, FH theory with $T_c^\infty=1300$ K and $b_0=1$ in the units used here; dashed line, density based on MP2 calculations of the all-*trans* molecular volume.

a significant increase of the average chain length regardless of the specific r_n value supporting our above premise. In addition to the simulation results the figure includes the theoretical dependence of n_c on μ^2 (corresponding to the solid lines in Fig. 3). The agreement between theory and simulation is qualitative. The theoretical n_c is plagued by a strong dependence on the details of the interaction between the Stockmayer particles. Quantitative agreement between theory and simulation can, for instance, be improved if an additional factor is introduced reducing the numerical value of ε_i in Eq. (25). However, this procedure does not yield additional physical insight beyond the level of the present one-parameter theory.

Finally, we want to draw a more explicit correspondence between the FH lattice description and an ordinary system of chain molecules at gas-liquid criticality. Figure 6 shows experimental critical point data for n-alkanes vs their number of methylene groups, n. The solid curves are well-known results following from the equation of state, Eq. (5) [4], i.e., $T_c=T_c^\infty n/(1+\sqrt{n})^2$ with $T_c^\infty=T_{Bolye}$, $\phi_c=1/(1+\sqrt{n})$, and P_c accordingly. We emphasize that this is not an attempt to de-

scribe the critical data for n-alkanes quantitatively. This has been done elsewhere [18–20]. In addition, corrections to the FH critical point shift at large n, where n is the monodisperse chain length in pure polymer systems or in polymer-solvent mixtures also have been discussed (e.g., [21,22]). Instead, the main purpose of Fig. 6 is to highlight similarities between the Stockmayer system near gas-liquid criticality and an ordinary fluid of linear polymer or polymerlike molecules.

Notice that T_c^∞ is not known for n-alkanes. In the literature a rather wide range of values is discussed, e.g., 1100 to 1700 K in Ref. [18]. Here we use $T_c^\infty = 1300$ K. Notice that the function $f_T(n)$ in Eq. (7) also approaches a constant value in the limit $n \to \infty$. It is the factor (12) that yields the μ^2 dependence of T_c in the Stockmayer system. In the case of ρ_c, now the critical mass density, we use $\rho_c = m_0^{(n)}/b_0^{(n)}\phi_c$ simply setting $m_0^{(n)}/b_0^{(n)} = 1$. Here $b_0^{(n)}$ is the volume per carbon subunit, and $m_0^{(n)}$ is its mass. The important point to note is that both quantities depend on n. This is demonstrated by the dashed line in the middle panel of Fig. 6. The line connects the values $(m_0^{(n)}/b_0^{(n)})/(m_0^{(1)}/b_0^{(1)})\rho_c^{methane}$ obtained for $n = 1, 2, \ldots, 6$ using the experimental critical density of methane. $m_0^{(n)}/b_0^{(n)}$ is obtained by dividing the mass of the respective n-alkane by its volume computed via the quantum chemistry program SPARTAN [23] using second-order Møller-Plesset (MP2) perturbation theory (6-31G^* basis set) applied to all-*trans* conformations (for $n > 4$). Notice that the initial rise of the critical density with n is the consequence of a shrinking volume per C subunit essentially due to dispersion attraction. This is the motivation to include the relation (26) into the above theory, even though the maximum exhibited by ρ_c in Fig. 3 is much less pronounced in comparison to the maximum of the critical mass density in Fig. 6. In order to extend the available data for ρ_c to larger n values we have assumed the relation $\rho_c = 6.718 n P_c/T_c$. Data values obtained via this relation are represented by the smaller dots. Notice that $P_c/(\rho_c T_c) = \text{const}$ is a fairly good approximation for $n \leqslant 18$, where ρ_c is known independently. For $n > 18$ the scatter is considerable. But the extrapolation suggests that the experimental ρ_c may decrease in reasonable accord with the FH prediction. Finally, the solid line in the bottom panel of Fig. 6 is plotted using $T_c^\infty = 1300$ K and $b_0 = b_0^{(n)} = 1$ allowing a rough comparison between the slope of P_c for large n as obtained experimentally in comparison to the FH result.

IV. CONCLUSION

In this work we develop a theory, based on the FH lattice description for polymer systems, to explain the dependence of the gas-liquid critical point in the Stockmayer fluid on dipole strength. The shift of the critical point to lower densities and higher temperatures as function of dipole strength, which has been observed in numerous computer simulations, closely resembles the critical point shift as function of chain length in ordinary linear polymer systems. The dependence of the critical temperature on dipole strength may be explained without particle association, but this explanation does not include the shift of the critical density. In particular, the decrease of the critical density with increasing dipole strength is a consequence of the existence of reversible chains near criticality. Contrary to the case of ordinary linear polymer systems, where the Flory approach yields a finite critical temperature for infinite chain length, the critical temperature continues to increase proportional to the square of the dipole moment even for large average chain length. In addition we do not find evidence, in neither simulation or theory, for an abrupt disappearance of the gas-liquid critical point found to occur in earlier simulation work. It is worth noting that the possible transition to ferroelectric liquid ordering is not expected to interfere with this conclusion (cf. Ref. [5]), a possibility that has been discussed in theories of phase behavior in dipolar fluids (e.g., [24,25]).

Finally we want to comment on the relation of this work to the defect-induced critical phase separation in dipolar fluids proposed by Tlusty and Safran [26]. The present approach does not include such defects, which amount to treating the system as reversible, random network with variable strand length including free ends and cross links. Thus far we do not have evidence for network formation from our MD simulations. However, cross links may be difficult to detect for small cross-link density. Nevertheless, the free energy in Eq. (2) can be extended by an elastic contribution to describe a random "polymer network" (e.g., Chapter 21 in Ref. [27]) and an appropriate defect energy contribution may be added. Without the latter the resulting equation of state closely resembles Eq. (5), where n becomes an average strand length, for large strand lengths. However, the additional energetic contribution will modify the equation of state and therefore the result shown in Fig. 3.

[1] P. I. C. Teixeira, J. M. Tavares, and M. M. Telo da Gama, J. Phys.: Condens. Matter **12**, R411 (2000).
[2] B. Huke and M. Lücke, Rep. Prog. Phys. **67**, 1731 (2004).
[3] P. G. de Gennes and P. A. Pincus, Phys. Kondens. Mater. **11**, 189 (1970).
[4] P. J. Flory, *Principles of Polymer Chemistry* (Cornell University Press, Ithaca, NY, 1953).
[5] J. Bartke and R. Hentschke, Mol. Phys. **104**, 3057 (2006).
[6] M. E. van Leeuwen and B. Smit, Phys. Rev. Lett. **71**, 3991 (1993).
[7] R. P. Sear, Phys. Rev. Lett. **76**, 2310 (1996).
[8] R. van Roij, Phys. Rev. Lett. **76**, 3348 (1996).
[9] M. J. Stevens and G. S. Grest, Phys. Rev. E **51**, 5976 (1995).
[10] J. Dudowicz, K. F. Freed, and J. F. Douglas, Phys. Rev. Lett. **92**, 045502 (2004).
[11] J. Dudowicz, K. F. Freed, and J. F. Douglas, J. Chem. Phys. **119**, 12645 (2003).
[12] The application of FH-like lattice theories to reversible chain assembly is not new. The application to phase separation in solutions of rodlike micelles is discussed by R. L. Scott, J.

Phys. Chem. **69**, 261 (1965); R. Kjellander, J. Chem. Soc., Faraday Trans. 2 **78**, 2025 (1982); and D. Blankschtein, G. M. Thurston, G. B. Benedek, J. Chem. Phys. **85**, 7268 (1986). Other early studies by Herzfeld and Briehl [R. W. Briehl and J. Herzfeld, Proc. Natl. Acad. Sci. U.S.A. **76**, 2740 (1979); J. Herzfeld and R. W. Briehl, Macromolecules **14**, 1209 (1981)] focused on the coupling between the variable length distribution and the isotropic-to-nematic transition in systems of rodlike reversible aggregates.

[13] P. B. Lenz and R. Hentschke, J. Chem. Phys. **121**, 10809 (2004).

[14] In Ref. [13] we discuss the mechanism of a possible decrease of the mean aggregate length at high solute volume fractions for certain combinations of the ε_{xy}.

[15] J. Bartke and R. Hentschke (unpublished) The details of the model potential and the molecular dynamics simulation algorithm are described [5, Sec. II] (in the case of vanishing polarizability).

[16] M. E. van Leeuwen, Mol. Phys. **82**, 383 (1994).

[17] J. Stoll, J. Vrabec, and H. Hasse, Fluid Phase Equilib. **209**, 29 (2003).

[18] E. D. Nikitin, High Temp. **36**, 305 (1998).

[19] E. W. Lemmon and A. R. H. Goodwin, J. Phys. Chem. Ref. Data **29**, 1 (2000).

[20] J. C. Pamies and L. F. Vega, Mol. Phys. **100**, 2519 (2002).

[21] H. Frauenkron and P. Grassberger, J. Chem. Phys. **107**, 9599 (1997).

[22] L. V. Yelash, T. Kraska, A. R. Imre, and S. J. Rzoska, J. Chem. Phys. **118**, 6110 (2003).

[23] Computer code SPARTAN '04 MACINTOSH (V1.0.3) (Wavefunction Inc., Irvine, CA).

[24] H. Zhang and M. Widom, Phys. Rev. E **49**, R3591 (1994).

[25] B. Groh and S. Dietrich, Phys. Rev. E **50**, 3814 (1994).

[26] T. Tlusty and S. A. Safran, Science **290**, 1328 (2000).

[27] T. L. Hill, *An Introduction to Statistical Thermodynamics* (Dover, New York, 1986).